JOURNAL OF AIRCRAFT
Vol. 31, No. 2, March–April 1994

Experimental Studies of Vortex Flaps and Vortex Plates

K. Rinoie* and J. L. Stollery†
Cranfield Institute of Technology, Bedford MK43 0AL, England, United Kingdom

Low-speed wind-tunnel tests have been made on a number of vortex flap and vortex plate configurations at the Cranfield Institute of Technology. The objectives of the experiment are to assess the benefits of these devices on the lift/drag ratio improvement of delta wings. The force and surface pressure measurements were made on a 1.15-m span, 60-deg delta wing model. Results indicate that the vortex flap deflection angle, which causes the flow to attach on the flap surface without any large separation, shows a much higher lift/drag ratio than the flap deflection angle which forms a leading-edge separation vortex over the flap surface. The performance of a vortex plate protruding from the leading edge of the datum delta wing is comparable to that of the vortex flap. However, when the vortex plate is used with the vortex flap deflected, it showed no benefit in these tests.

Nomenclature

b = local span, m
C_D = drag coefficient
C_{D0} = C_D at zero lift
C_L = lift coefficient
C_m = pitching moment coefficient nondimensionalized using Cr and measured about $x/Cr = 0.4$
Cp = pressure coefficient
Cr = wing centerline chord, m
g = vortex plate leading-edge position measured from leading edge of the wing in the chordwise direction, m
L/D = lift/drag ratio
Re_{Cr} = Reynolds number based on wing centerline chord
U_∞ = freestream velocity, m/s
x = chordwise coordinate measured from the apex of the delta wing, m
y = spanwise coordinate orthogonal to x, measured from the wing centerline, m
α = wing incidence, deg
α_g = geometrical wing incidence (i.e., without tunnel corrections), deg
δ_f = vortex flap deflection angle measured normal to the hinge line, deg

Introduction

A DELTA wing is often used as a main wing for the aircraft such as the next generation, high-speed civil transport aircraft. It is known that the L/D ratio of the delta wing at low speeds is relatively poor. Therefore, the improvement of L/D ratio is an essential factor for improving the takeoff and climb performance of delta wing aircraft. The leading-edge vortex flap[1] and the vortex plate[2] have been proposed to improve the aerodynamic efficiency of delta wings at low speeds.

The leading-edge vortex flap (LEVF) is a full span deflectable surface at the leading-edge of a delta wing. With the flap deflected downward, a leading-edge separation vortex may be formed over the forward facing flap surface (Fig. 1). The suction force generated by the vortex acts on the flap surface and generates a thrust component. Hence, the drag is reduced and the L/D ratio improved. Many tests have been made and confirm that the LEVF can improve the low-speed aerodynamic efficiency of delta wings. Reference 3 gives an overview of LEVF research.

The vortex plate is similar to a forward facing split flap. This vortex plate is a thin plate attached to the lower surface of the leading-edge of the delta wing (Fig. 2a). With the plate fitted, a leading-edge cavity is formed between the delta wing and the vortex plate. Reference 2 suggested that at positive incidence the flow separates at the plate leading edge and forms a spanwise vortex which induces a suction over the cavity surface. Therefore, the plate creates some leading-edge thrust and the drag is reduced.

In order to investigate the flow around the LEVF at the maximum L/D condition and to understand how the vortex plate works, some earlier tests were made using the 60-deg delta wing fitted with vortex flaps[4,5] and vortex plates[5] at the College of Aeronautics, Cranfield Institute of Technology. The results are summarized below:

1) At the incidence when the L/D ratio reaches a maximum, the flow attaches on the flap with no large vortex being formed.

2) At high incidences, a leading-edge separation vortex is formed on the LEVF surface. Because of the suction effect of this vortex, the L/D is higher than that of the datum wing, as was suggested in Ref. 1.

3) By fitting a vortex plate to the basic wing (no LEVF), the L/D ratio for all ranges of C_L greater than 0.3 is significantly improved. A better performance was obtained with the vortex plate protruding ahead of the leading edge of the wing (Fig. 2b).

In Ref. 5, the flat plate wing model had beveled leading edges. These beveled edges might have affected both the separation position and the formation of the leading-edge separation vortex. Therefore, it is of interest whether the conclusions of Ref. 5 are applicable to the other wing having different cross sections. In this article, further tests are conducted using a 1.15-m span, 60-deg delta wing model, which is the same one that was used in Ref. 4. A symmetrical smooth convex shape is used for the cross section of this model in order to avoid any undesirable separation on the wing surface.

These previous studies[4,5] concentrated on incidences up to about 30 deg, because the emphasis was on finding the maximum L/D ratios. These values occurred at rather low lift coefficients. Reference 4 showed that the LEVF was still giving some L/D improvement at the highest incidence tested. In practice, any benefit at high incidence may be useful.

Presented as Paper 92-4101 at the 18th International Council of the Aeronautical Sciences Congress, Beijing, People's Republic of China, Sept. 20–25, 1992; received Nov. 9, 1992; revision received Jan. 22, 1993; accepted for publication Jan. 22, 1993.

*Visiting Research Fellow; currently Associate Professor, Department of Aeronautics and Astronautics, Faculty of Engineering, University of Tokyo, 7-3-1 Hongo, Bunkyo-Ku, Tokyo, 113 Japan.

†Professor of Aerodynamics, College of Aeronautics. Fellow AIAA.

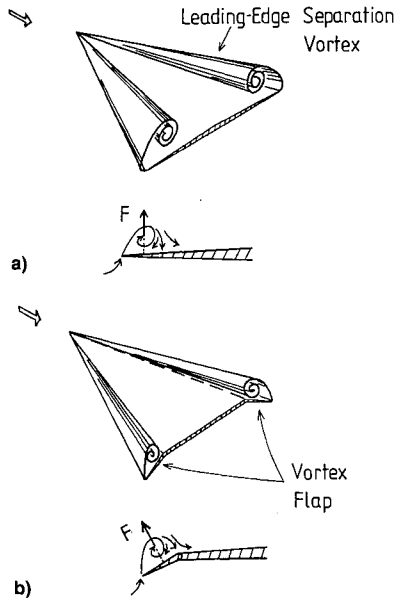

Fig. 1 Concept of vortex flap: a) flat delta wing and b) delta wing with LEVF deflected.

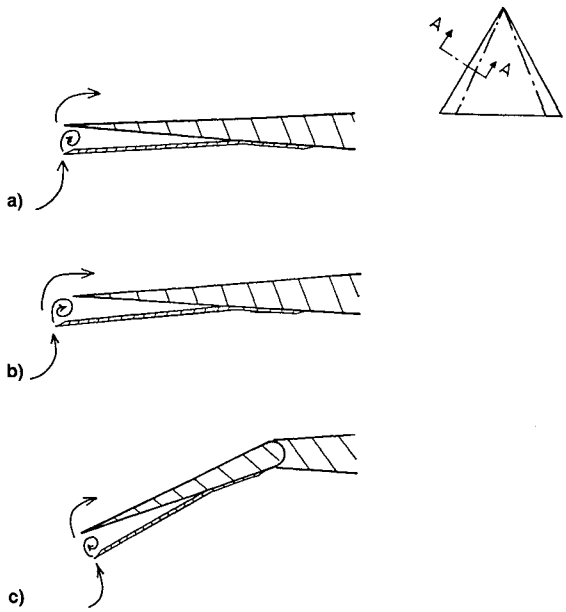

Fig. 2 Concept of vortex plate: a) flat delta wing with vortex plate, b) flat delta wing with protruding vortex plate, and c) delta wing with vortex plate when LEVF is deflected.

In Ref. 5, the vortex plate was attached to the delta wing without flaps deflected. However, when the vortex plate is attached to the deflected vortex flap as shown in Fig. 2c, the drag reduction will be caused by the effect of combining the vortex flap and the vortex plate. There may be some beneficial effects on wing performance.

In the present study, further tests were conducted in the Cranfield 2.4- × 1.8-m low-speed wind tunnel. The force and surface pressure measurements were made on the delta wing model with the LEVF alone, with the vortex plate alone, and with the vortex flap/vortex plate combination. Measurements of the LEVF alone were done in the incidence range of −8 to 57 deg. Other measurements were done in the incidence range of −8 to 32 deg. All tests were done at a side slip angle of 0 deg, and at a tunnel speed of U_∞ = 30 m/s.

In summary, the purpose of this study is to gain more understanding of the complex flows around the delta wing with vortex flaps up to incidences of about 60 deg, to confirm the flow conditions giving the maximum L/D ratio of the wing with vortex flaps, and to investigate the benefits of the vortex plate, with and without flaps deflected.

Experimental Details

Figure 3 shows the model details. The model is a 60-deg delta wing with sharp leading edge and trailing edges. The Cr is 1.0 m. The aerofoil section at centerline is a symmetrical, smooth convex shape described by the form

$$\frac{y}{Cr} = \pm\frac{x}{8Cr}\left(1 - \frac{x}{Cr}\right)\left(1 - \frac{x}{2Cr}\right)$$

The maximum thickness/chord ratio is 4.8%. The spanwise thickness distribution varies linearly from centerline to tip. The model has the LEVF hinge lines running from the wing apex to 75% of the trailing-edge semispan station. Two rows of pressure tappings were located on the upper surface.

Different flap deflections of δ_f = 0–60 deg were tested in Ref. 4. It was concluded that the δ_f = 30-deg case has the best performance for a wide C_L range. In order to check the repeatability of measurements in Ref. 4, and in order to measure the flap performance at high incidences greater than 30 deg, the datum wing (δ_f = 0-deg) and δ_f = 30-deg cases were again tested here. Nine different flap deflections of δ_f = 0–60 deg were tested to determine the maximum L/D condition for each flap setting.

Two different types of vortex plates were tested in this experiment. The first type (Fig. 4a) is similar to the one used in Ref. 5. The plate was attached to the lower surface of the datum model (no LEVF deflection). The plate was bent as shown in Fig. 4a so that the distance between the leading edge of the plate and that of the wing was 10 mm at every spanwise station in side view. The plate can be moved forward, as shown in Fig. 4a. The position of the plate is defined by the chordwise distance g between the leading edge of the wing and that of the vortex plate. In these tests the plate was set at g/Cr = 0 and 0.02. The vortex plate described above is called the "parallel" vortex plate.

A second type of vortex plate was made in order to check the effect combining the vortex plate and the vortex flap. The

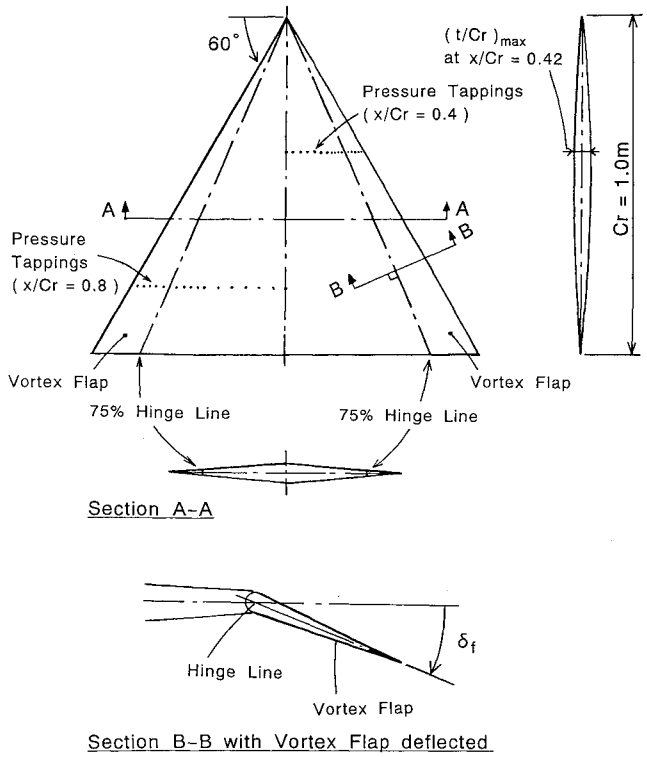

Fig. 3 Delta wing model with LEVF.

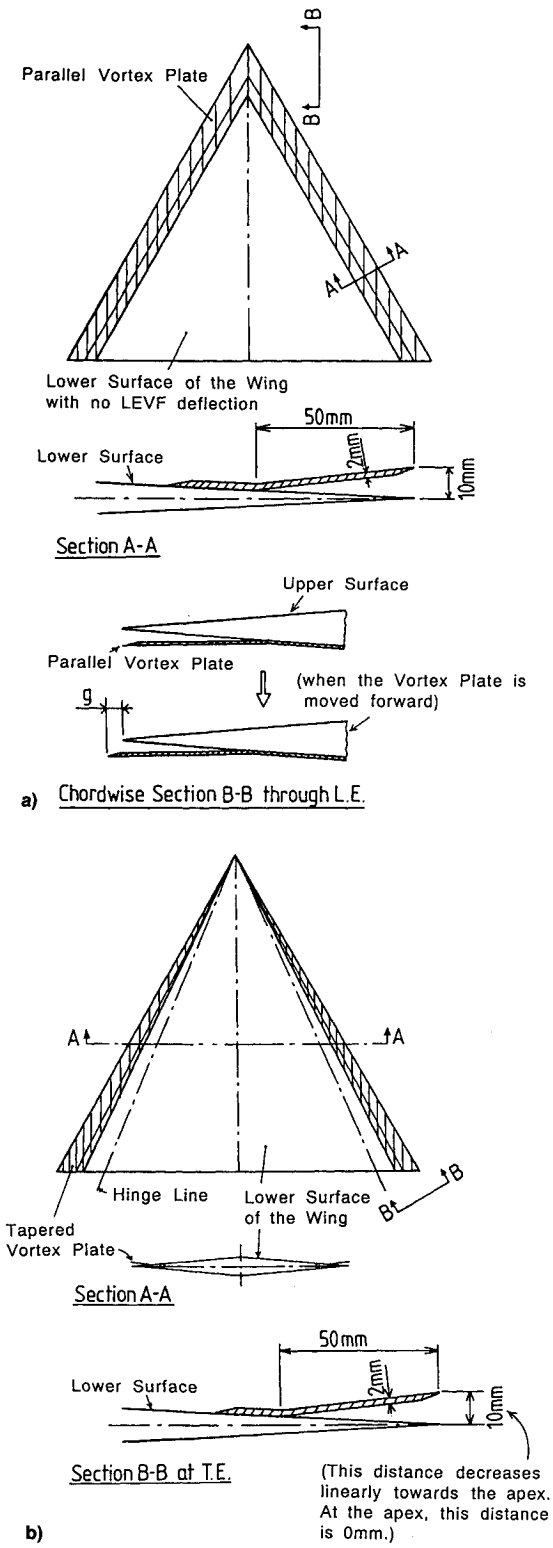

Fig. 4 Delta wing model with vortex plate: a) parallel vortex plate and b) tapered vortex plate.

plan shape is smaller than the vortex flap, as shown in Fig. 4b, so that the vortex flap is deflectable. The distance between the leading edge of the plate and that of the wing in side view is 10 mm at the trailing edge of the wing. This distance decreases linearly towards the apex of the wing. At the apex this distance is zero. The leading edge of the plate coincides with that of the wing in plan view. The measurements were done without flaps deflected (δ_f = 0 deg) and with a δ_f of 30 deg. This vortex plate is hereafter referred to as the "tapered" vortex plate.

The experiments were made in the Cranfield 2.4- × 1.8-m low-speed, closed working section, closed return wind tunnel. All tests were done at a tunnel speed of U_∞ = 30 m/s. The Reynolds number based on the wing centerline chord was 2 × 10^6. The model was mounted inverted from the overhead balance by a single shielded strut and a tail wire. For measurements over the incidence range of −8 to 32 deg, the model was mounted at the centerline of the tunnel. However, it was impossible to set the model at an incidence above 45 deg in this way. Therefore, an extended center strut and an extended curved tail strut were used for measurements in the incidence range of 30–57 deg.

Lift, drag, and pitching moments were measured using the overhead six-component electromechanical balance. Tunnel boundary corrections were applied to the measured data. Interference between the strut and the model was not accounted for. Since the tunnel boundary corrections used here are only suitable for low incidences, the results obtained here at high incidences must be treated with caution. All aerodynamic coefficients were calculated based on the constant datum delta wing area. In order to measure surface pressure distributions, a "Scanivalve" was mounted within the model. Further experimental details can be found in Ref. 6.

Results and Discussion

Vortex Flap

Figure 5 shows the C_L vs α curves for the datum wing and the δ_f = 30-deg case. Results which were obtained using the low incidence rig and the high incidence rig are shown in the same figure. The two sets of results connect "smoothly" at about α = 30 deg. At zero incidence, the C_L of the datum wing is slightly negative. Since the model is symmetrical, the C_L should be zero. The reason why the C_L showed a negative value at α = 0 deg is thought to be due to the presence of the shielded strut. Figure 5 shows that deflecting the LEVF downwards moves the whole C_L-α curve to the right. Therefore, the zero lift incidence and the stall angle are increased, while the C_L at a constant incidence (below the stall) is reduced.

In Fig. 5, a comparison is made with other experimental results from tests on a flat delta wing. In Ref. 7, measurements were made using a 0.92-m span, 60-deg delta wing at a Reynolds number of 2.37 million. This model had a 12% biconvex section, which is quite similar in shape to that of the present model. The results from the 12% biconvex wing tests are very similar to those of the datum wing tested here.

The C_D-α curves (Fig. 6) show the same trend, the whole curve being moved to higher values of incidence. The 12% biconvex wing[7] shows larger C_D values than the present results at low incidences, but this difference is reversed at the higher incidences. Drag is known to be sensitive to the section profile.

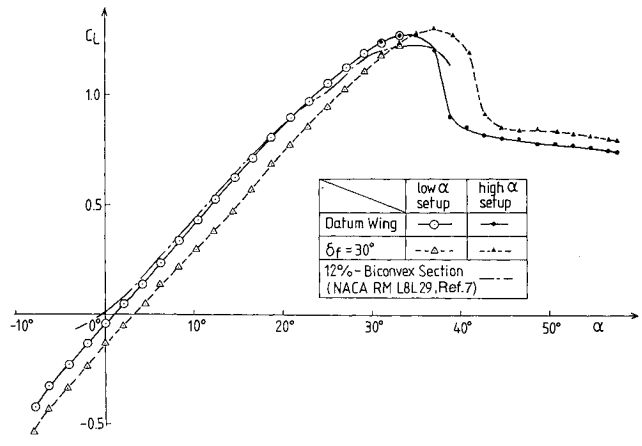

Fig. 5 Effect of LEVF on C_L vs α.

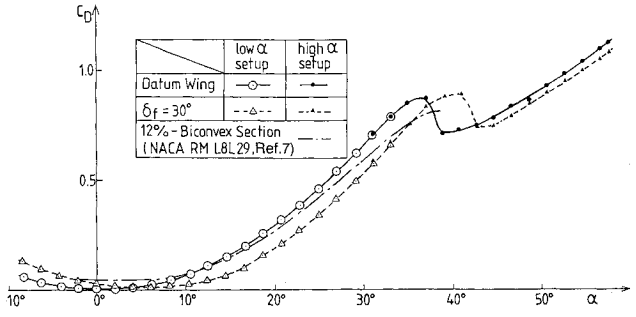

Fig. 6 Effect of LEVF on C_D vs α.

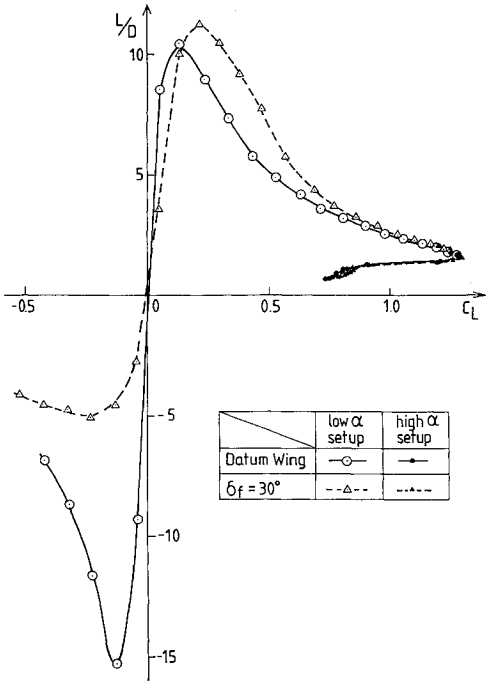

Fig. 7 Effect of LEVF on L/D vs C_L.

Figure 7 shows L/D vs C_L. The $(L/D)_{max}$ for a flap deflection of 30 deg is increased from the datum wing value of 10.4–11.3. For the datum wing, the L/D at negative lift is higher than that for positive lift. Again, any lack of symmetry is probably due to strut interference. A large L/D improvement for δ_f = 30 deg is seen at about C_L = 0.25–0.5. The greatest percentage improvement in the L/D ratio for δ_f = 30 deg is about 40% at a C_L of 0.45. However, after the stall the δ_f = 30-deg tests show that there is no benefit in using a LEVF.

Figure 8 shows the pitching moment curves measured about the model mounting point x/Cr = 0.4 for all tests, including the vortex plate results. The LEVF has little effect on C_m. The C_m-C_L curves are roughly linear before the stall. The C_m values at C_L = 0 are zero for the datum and the δ_f = 30-deg cases. The aerodynamic center position measured from the C_m-C_L slope is $0.57Cr$.

These present results (Figs. 5–7) and the previous results in Ref. 4 (which were made at incidences up to 30 deg) agree well.

Figure 9 shows surface pressure distributions for the upper surface, the datum, and the δ_f = 30-deg cases. Measurements were made at x/Cr = 0.4 and 0.8. Results at x/Cr = 0.8 were similar to those at x/Cr = 0.4, apart from low suction peaks at high incidences which were caused by vortex breakdown. Only the x/Cr = 0.4 results are shown in this article.

Figure 9a shows the Cp distributions for the datum wing. At α = 6.2 deg, the features of a leading-edge separation vortex are clearly recognizable. There is a flat Cp area at the tip of the wing between $y/(b/2)$ = 0.91 and 0.95 ($Cp \cong -0.6$) which shows the existence of a secondary separated flow. At

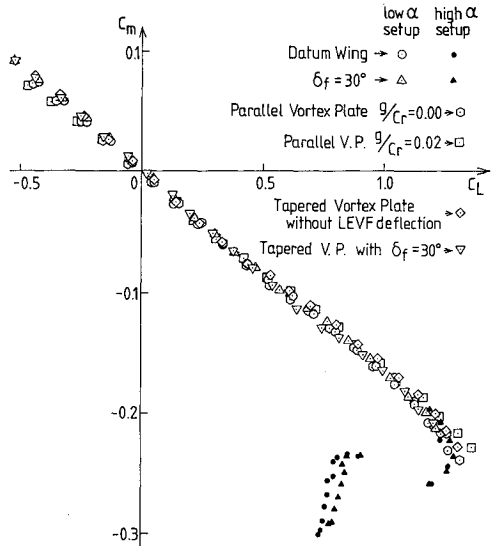

Fig. 8 Effect of LEVF and vortex plate on C_m vs C_L.

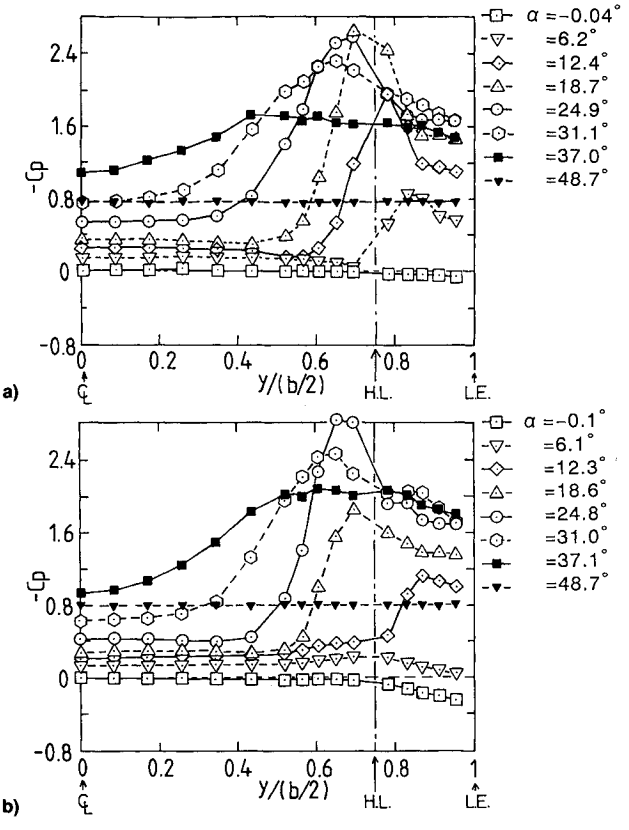

Fig. 9 Surface pressure distributions for a) datum wing at x/Cr = 0.4 and b) δ_f = 30 deg at x/Cr = 0.4.

α = 12.4, 18.7, and 24.9 deg, there is a large leading-edge separation vortex on the wing with high peak suctions. By α = 37.0 deg, the Cp distribution shows that the vortex suction has decreased, but spread out to cover half the local wing span. This may signify vortex breakdown. At α = 48.7 deg, the Cp distribution is completely flat. This suggests that the vortex type of flow has collapsed and that the flow is now totally separated over the top surface of the wing.

Figure 9b shows the Cp distributions for the wing with δ_f = 30 deg. At α = 6.1 deg, there is no vortex formation, and this suggests that the flow attaches on the flap surface without any large separation. At α = 12.3 deg, a suction region is seen on the flap [$y/(b/2)$ = 0.75–1.0]. There is no flat Cp area at the tip of the wing, which means that there is no

secondary separation. Although the flow visualization tests were not done in this experiment, the suction peak value measured in this region ($Cp \cong -1.1$) is larger than that of the leading-edge separation vortex at $\alpha = 6.2$ deg for the datum wing (Fig. 9a). This seems to indicate the presence of a separation vortex at this region. The spanwise length of this vortex at $\alpha = 12.3$ deg is almost the same as the flap span. At $\alpha = 18.6$ deg, a secondary separation occurs inside the leading-edge separation vortex. At $\alpha = 24.8$ deg, the suction caused by the vortex reaches its maximum value. After the stall ($\alpha > 37.1$ deg), the Cp shows a flat distribution suggesting that the flow has totally separated from the wing surface. Therefore, there was no benefit in L/D results for the $\delta_f = 30$-deg case after stall (Fig. 7).

Effect of δ_f on L/D at Constant Incidence

In order to find the condition which gives the maximum L/D, some measurements were made by changing δ_f at constant incidence. Flap angles were varied between 0–60 deg at fixed incidence values of 6, 8, 10, 12, and 14 deg. Force measurements and surface pressure measurements were made under these conditions. The incidences, as corrected for tunnel wall interference, are different for every flap deflection angle. Therefore, α_g as measured from the tunnel centerline is used in this section to define the incidence angle.

Figure 10 shows L/D vs δ_f at different incidences. This shows that at $\alpha_g = 6$ deg, the L/D attains a maximum with $\delta_f = 20$ deg. As the incidence increases, the maximum L/D decreases and the δ_f at which $(L/D)_{max}$ is achieved, increases.

Figure 11 shows the measured pressure distributions for $\alpha_g = 6$ and 12 deg at $x/Cr = 0.4$. Different δ_f results (at constant α_g) are shown in each figure. At $\alpha_g = 6$ deg (Fig. 11a), the L/D attains its maximum at $\delta_f = 20$ deg. At this flap deflection angle there is a small suction region at the leading edge of the upper surface [$y/(b/2) = 0.9$–1.0]. On the lower flap surface at $\delta_f = 20$ deg, there is no separation. At $\delta_f = 25$ deg, there is no separation region on either surface. At $\alpha_g = 6$ deg, as δ_f decreases below $\delta_f = 20$ deg, so the spanwise length of the separation bubble on the top surface increases. At $\delta_f = 0$ deg, secondary separation occurs at $y/(b/2) \cong 0.9$ on the upper surface, and a leading-edge separation vortex has formed over the wing [$y/(b/2) = 0.7$–1.0]. As δ_f increases beyond 20 deg, separation occurs at the flap hinge line [$y/(b/2) = 0.75$], and a separation region is formed inboard of that line [see, e.g., $\delta_f = 40$ deg, $y/(b/2) = 0.6$–0.75].

At $\alpha_g = 12$ deg (Fig. 11b), the L/D attains its maximum at $\delta_f = 30$ deg. At this flap deflection angle the leading-edge separation vortex is formed on the flap upper surface [$y/(b/2) = 0.75$–1.0] and its reattachment line almost coincides with the flap hinge line (as was also shown in Fig. 9b). As δ_f decreases below $\delta_f = 30$ deg, the spanwise length of the separation vortex increases as it did at the lower incidence ($\alpha_g = 6$ deg). As δ_f increases above $\delta_f = 30$ deg, the separation

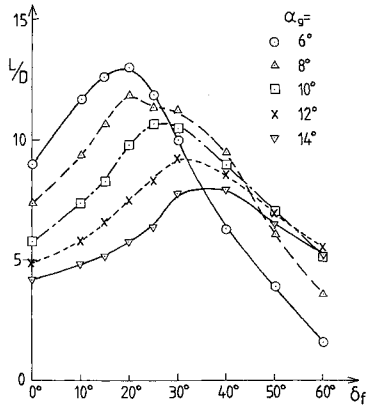

Fig. 10 L/D vs δ_f at constant α_g.

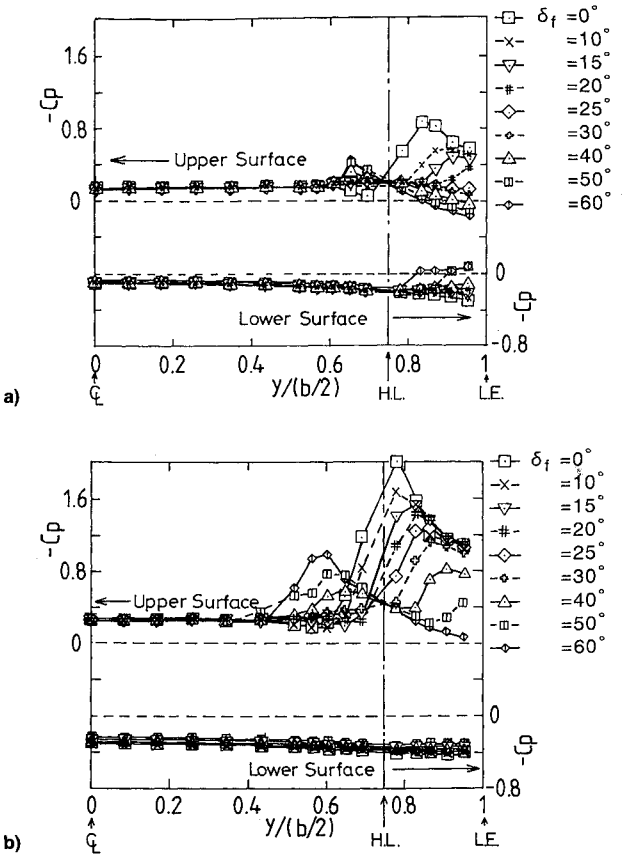

Fig. 11 Surface pressure distributions at constant incidence for a) $\alpha_g = 6$ deg at $x/Cr = 0.4$ and b) $\alpha_g = 12$ deg at $x/Cr = 0.4$ (upper and lower surfaces).

region is formed not only on the flap surface, but also inboard of the flap hinge line [e.g., $\delta_f = 40$ deg, $y/(b/2) = 0.8$–1.0 and $y/(b/2) = 0.5$–0.75]. At $\delta_f = 60$ deg, the vortex on the flap surface disappears and the only vortex formed is inboard of the flap hinge line [$y/(b/2) = 0.4$–0.75].

Figure 12 shows C_D vs C_L curves at constant incidence ($\alpha_g = 6$ and 12 deg, Fig. 12b), together with the corresponding flow pattern sketches in the transverse plane at $x/Cr = 0.4$ (Fig. 12a). These flow pattern sketches were deduced from the pressure measurements. The C_D vs C_L curves in Fig. 12b show that the C_L increases as the δ_f decreases at constant incidence, and that the L/D ratio attains its maximum near the point where C_D is a minimum.

At the smaller incidence ($\alpha_g = 6$ deg), Fig. 12a shows that a large leading-edge separation vortex is formed on the flap surface when the flap deflection angle is zero ($\delta_f = 0$ deg). Because of the suction effect of this vortex, the C_D, shown in Fig. 12b, has a large value at $\delta_f = 0$ deg. Figure 12a also shows that at a flap deflection angle of 20 deg, only a small separation bubble is formed on the flap, and at $\delta_f = 25$ deg, no bubble is formed at all. Since the flow attaches on the flap without any large separation, the C_D in Fig. 12b has a much smaller value at $\delta_f = 25$ deg than that at $\delta_f = 0$ deg. Further increase of δ_f causes the flow to separate at the flap hinge line, and a separated region is formed inboard of the hinge line ($\delta_f = 40$ and 60 deg at $\alpha_g = 6$ deg in Fig. 12a). Primarily, because of this separated region inboard of the hinge line, the C_D of the $\delta_f = 40$- and 60-deg configurations in Fig. 12b have greater values than those of the $\delta_f = 20$- and 25-deg cases.

At the larger incidence of 12 deg, for both small δ_f ($\delta_f = 15$ deg) and large δ_f ($\delta_f = 60$ deg), Fig. 12a shows the flow is similar to the patterns drawn for $\alpha_g = 6$ deg. However, when the L/D attains its maximum value ($\delta_f = 30$ deg), Fig. 12a shows that the leading-edge separation vortex is formed entirely over the flap surface, and the flow reattaches near

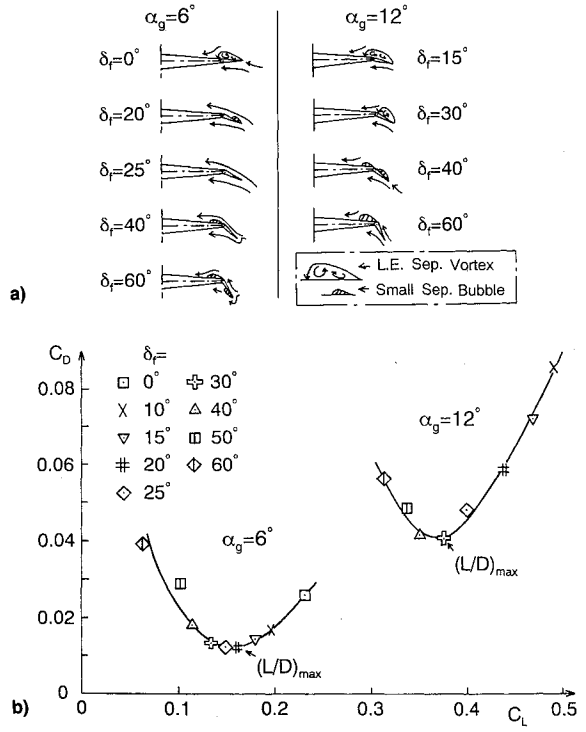

Fig. 12 Effect of δ_f on C_D vs C_L and on flow patterns at α_g = 6 and 12 deg: a) crossflow patterns and b) C_D vs C_L.

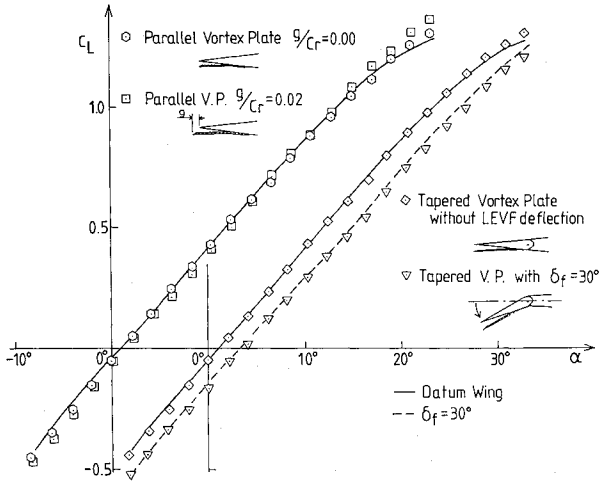

Fig. 13 Effect of vortex plate on C_L vs α.

the flap hinge line. Because the vortex is formed only on the LEVF surface and the suction force of this vortex acts perpendicular to the deflected flap, the C_D in Fig. 12b shows a smaller value at δ_f = 30 deg than those at other δ_f smaller than 30 deg, as was explained in section 1.

The $(L/D)_{max}$ at α_g = 6 deg is larger than that at α_g = 12 deg, as was shown in Fig. 10. This implies that the highest L/D is attained when the flow attaches on the flap surface without any large separation. A similar conclusion was reached in Ref. 5 where the wing model has a different cross section (beveled edges) to the present model. This highest L/D ratio is reached at a small value of C_L. If a larger C_L is needed from a given configuration, then a larger incidence is needed, and the best L/D that can be achieved appears to be with the leading-edge vortex entirely on the flap and reattachment near the hinge line.

Vortex Plate

Figure 13 shows the C_L vs α curves for parallel and tapered vortex plates together with the datum wing and δ_f = 30-deg tests. In this section, the results of the vortex plate tests in the figures are not connected by lines in order to distinguish them from the results of the datum wing and δ_f = 30-deg results. This shows that the effects of either the parallel or the tapered vortex plates on lift are quite small.

Figure 14 shows the C_D vs α curves. At incidences greater than 8 deg, the drag with the parallel vortex plate fitted (Fig. 14a) is smaller than the datum wing. The drag of the tapered vortex plate without LEVF deflection (Fig. 14b) is smaller than that of the datum wing. The drag of the tapered vortex plate with δ_f = 30 deg is smaller than that of the LEVF alone (δ_f = 30 deg). The drag reductions of the tapered vortex plates are most significant at the higher incidences.

Figure 15 shows the L/D ratio vs C_L. For the case of the parallel vortex plate with g/Cr = 0 (Fig. 15a), although the maximum value of L/D is reduced in comparison with the datum wing, the L/D ratio is improved for all C_L values greater than 0.4. For the case of the parallel vortex plate with g/Cr = 0.02 (Fig. 15a), the maximum value of L/D is almost the same as that of the datum wing, but it is achieved at a larger value of C_L. The L/D ratio is better with the vortex plate fitted for all values of C_L greater than 0.2. In comparison with the LEVF results, the L/D for g/Cr = 0.02 is roughly similar to that of the δ_f = 30 deg at positive C_L, although the maximum value is somewhat smaller (Fig. 7). For the tapered vortex plate without LEVF deflection (Fig. 15b), the maximum value of L/D is smaller than that of the datum wing. The L/D ratio is slightly improved for C_L values greater than 0.3 when compared with results for the datum wing. This is caused by the drag reduction as was seen in Fig. 14. For the tapered vortex plate with δ_f = 30 deg (Fig. 15b), there is no benefit at any C_L value.

The C_m distributions for parallel and tapered vortex plates in Fig. 8 show that the parallel and tapered vortex plates have little effect on C_m, as was found for the LEVF.

Figures 16a and 16b show surface pressure distributions for the upper surface of the parallel vortex plate (g/Cr = 0.02), and that of the tapered vortex plate with δ_f = 30 deg at x/Cr = 0.4. Figure 16a shows that there is only a small separation region at α = 6.2 deg on the wing, although a leading-edge separation vortex is formed on the datum wing at the same incidence as was shown in Fig. 9a. Increasing the incidence to 12.4 deg, there is a leading-edge separation vortex on the wing, but the spanwise length of this vortex is about 10% shorter than that on the datum wing at the same incidence (Fig. 9a), and there is no secondary separation. These results suggest that onset of the leading-edge separation vortex is delayed by the vortex plate g/Cr = 0.02. Figure 16b shows Cp distributions for the

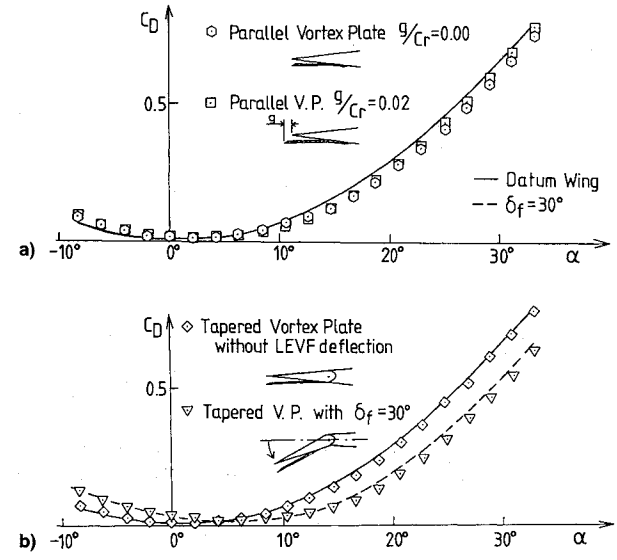

Fig. 14 Effect of vortex plate on C_D vs α: a) parallel vortex plate and b) tapered vortex plate.

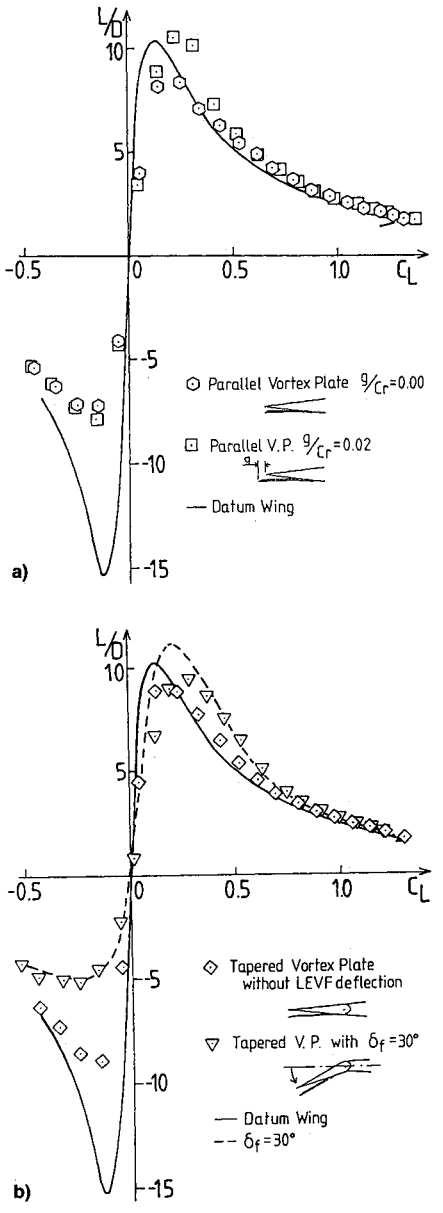

Fig. 15 Effect of vortex plate on L/D vs C_L: a) parallel vortex plate and b) tapered vortex plate.

tapered vortex plate with $\delta_f = 30$ deg. It is seen that the spanwise length of the leading-edge separation vortex at incidences 12.3 and 18.5 deg, is shorter than that of the $\delta_f = 30$-deg case at the same incidences (Fig. 9b).

Leading-Edge Suction

In this section, the leading-edge suctions recoverable through vortex flap and vortex plate deployments are discussed. The drag of a flat plate wing with no leading-edge suction is

$$C_D = C_{D0} + C_L \tan \alpha$$

where C_{D0} depends on the surface skin friction and the form drag. Using the measured C_L and C_{D0}, C_D assuming 0% leading-edge suction is calculated from the above formula and is plotted on the C_D vs C_L curves together with the measured data in Figs. 17a–d.

In contrast, a wing with a well rounded leading edge can show a large drag reduction due to leading-edge suction. In order to give some idea of the magnitude of this leading-edge suction, experimental data taken from Ref. 8 for a wing with a well rounded leading-edge are also plotted (Figs. 17a and 17b). In Ref. 8, measurements were made using a 0.91-m span, 60-deg

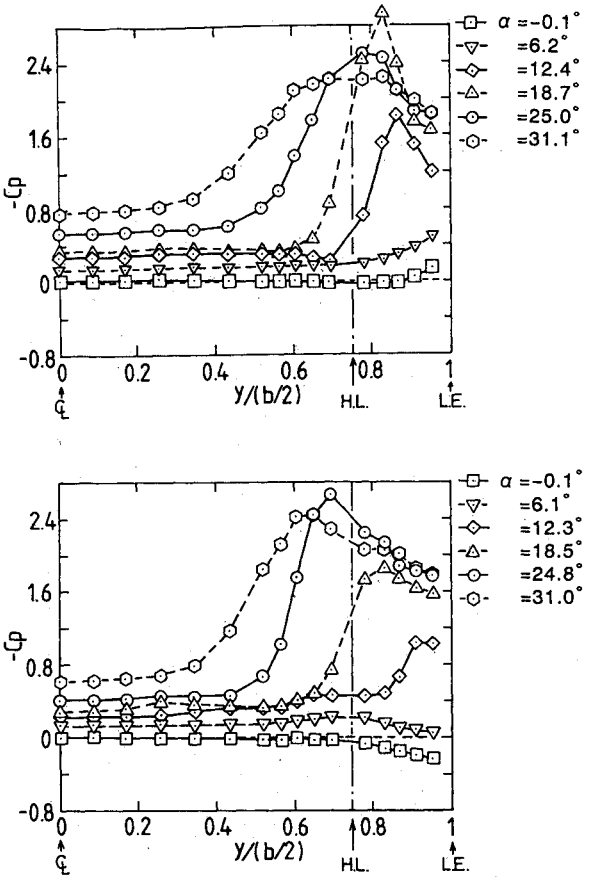

Fig. 16 Surface pressure distributions for a) parallel vortex plate $g/Cr = 0.02$ at $x/Cr = 0.4$ and b) tapered vortex plate with $\delta_f = 30$ deg at $x/Cr = 0.4$.

delta wing which had a 10% thickness ratio aerofoil section at a Reynolds number of 18.6 million (based on the root chord). The nose radius was 0.69% of the chord length.

Figure 17a shows the results for our datum wing. The measured drag polar shows almost the same value as that of the 0% leading-edge suction estimate at all incidences. This confirms that the datum wing with a sharp leading edge develops no leading-edge suction force.

Figure 17b shows the drag results for the wing with the LEVF deflected 30 deg. The measured value is considerably less than that estimated assuming zero leading-edge suction for all incidences. When compared with the rounded leading-edge data,[8] it can be seen that the vortex flap achieves a significant amount of C_D reduction.

The results for the parallel vortex plate $g/Cr = 0.02$ (Fig. 17c) show that the measured drag value is less than that for the zero leading-edge suction estimate at all positive incidences. This means that some leading-edge suction is recovered by incorporating a vortex plate. It is not clear that this C_D reduction is caused by the suction effect of a separation vortex between the leading-edge of the wing and that of the vortex plate as was suggested in Ref. 2. Smoke visualization tests, made on a different model with vortex plates in Ref. 5, did not confirm the existence of this vortex. It may be that the suction force is produced by the separated flow acting on the forward facing region between the wing and the vortex plate. Because of this, the C_D is reduced (as was shown in Fig. 14), and the L/D improved for C_L values greater than 0.2 (as was shown in Fig. 15).

The decrease in L/D ratio for small values of C_L (Fig. 15) is probably due to differences in the values of C_{D0}. The C_{D0} of the parallel vortex plate configuration is larger than that of the datum wing because of the difference of the forward facing area. Since a small increase in C_D causes a large decrease in L/D ratio at low values of C_L, the result is a reduction in the L/D values

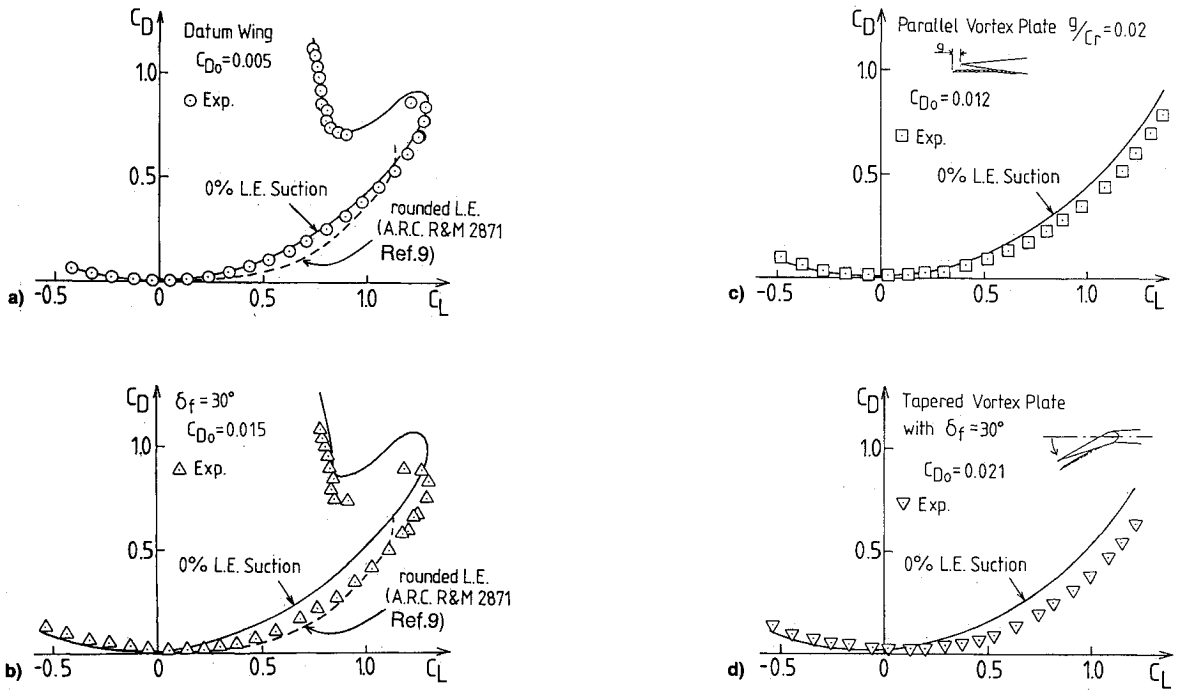

Fig. 17 Effect of leading-edge suction force on C_D: a) datum wing, b) δ_f = 30 deg, c) parallel vortex plate, and d) tapered vortex plate.

for the wing fitted with parallel vortex plates, as shown in Fig. 15.

When compared with the results of the tapered vortex plate with 30-deg LEVF deflection (Fig. 17d) and those of the LEVF alone (Fig. 17b), the C_D reduction is almost the same. The vertical distance between the leading edge of the wing and the vortex plate is 10 mm as measured at the wing tip. This is the same as for the parallel vortex plate. However, this gap decreases towards the apex as shown in Fig. 4. Therefore, the total forward facing area between the tapered vortex plate and the wing is smaller than that for the parallel vortex plate. The leading-edge suction acting on a smaller area gives a smaller drag reduction. Furthermore, the C_{D0} is larger than that of the LEVF (δ_f = 30 deg) alone. The result is that the maximum L/D of the tapered vortex plate with δ_f = 30 deg is smaller than that of the LEVF alone, as seen in Fig. 15.

In this article, vortex flap/vortex plate combination with a sharp leading edge showed no significant improvement in L/D ratio. However, such a combination may be more effective with a blunt leading-edge vortex flap which generates a weaker vortex by itself.

Conclusions

Measurements were made using the model having smooth convex shape in order to investigate the vortex flaps and the vortex plates.

1) The improvements in lift/drag ratio obtained by deflecting a leading-edge vortex flap were confirmed. The greatest percentage improvement in the lift/drag ratio is about 40% at a lift coefficient of 0.45 for a vortex flap deflection of 30 deg.

2) There is no benefit from the vortex flap at incidences higher than the stalling incidence.

3) The highest value of lift/drag ratio is achieved using a modest flap deflection angle with the wing at, or close to, the rather small incidence for which the flow attaches on the flap without any large separation.

4) At incidences higher than in 3, the lift/drag ratio reaches a local maximum when the vortex flap is deflected, so that a leading-edge separation vortex is formed on the vortex flap top surface with the reattachment line coincident with the flap hinge line. However this "local" value of maximum lift/drag ratio is smaller than that in 3.

5) The lift/drag ratio of the basic wing (no vortex flap) is improved by incorporating a parallel vortex plate, especially when the plate protrudes ahead of the leading edge of the wing. The improvement measured here was comparable to that obtained from a vortex flap deflection of 30 deg.

6) The tapered vortex plate with or without the vortex flap deflected showed no significant improvement in lift/drag ratio.

7) There is very little change of pitching moment for any of the leading-edge devices tested here.

Acknowledgments

We would like to thank K. P. Garry and members of the aerodynamics department workshop in Cranfield for their help in performing the wind-tunnel experiments. We also express our appreciation to P. B. Earnshaw, Royal Aerospace Establishment, Farnborough, England, for his advice and help in supporting this research.

References

[1]Rao, D. M., "Leading Edge Vortex-Flap Experiments on a 74 deg. Delta Wing," NASA CR-159161, Nov. 1979.

[2]Rao, D. M., and Johnson, T. D., Jr., "Investigation of Delta Wing Leading-Edge Devices," *Journal of Aircraft*, Vol. 18, No. 3, 1981, pp. 1051–1056.

[3]Campbell, J. F., and Osborn, R. F., "Leading-Edge Vortex Research: Some Nonplanar Concepts and Current Challenges," *Vortex Flow Aerodynamics Volume I*, NASA CP-2416, July 1986, pp. 31–63.

[4]Stollery, J. L., and Ellis, D. G., "The Behaviour and Performance of Leading-Edge Vortex Flaps," *Proceedings of 16th Congress of the International Council of the Aeronautical Sciences* (Jerusalem), Aug. 1988, pp. 758–765 (ICAS-88-4.5.2).

[5]Rinoie, K., "Experiments on a 60° Delta Wing with Vortex Flaps and Vortex Plates," *The Aeronautical Journal*, Vol. 97, No. 961, 1993, pp. 33–38.

[6]Rinoie, K., and Stollery, J. L., "Experimental Studies of Vortex Flaps and Vortex Plates Part. 2 1.15 m Span 60 deg Delta Wing," College of Aeronautics Rept. No. 9205, Cranfield Inst. of Technology, Bedford, England, UK, March 1992.

[7]Jaquet, B. M., and Brewer, J. D., "Low-Speed Static-Stability and Rolling Characteristics of Low-Aspect-Ratio Wings of Triangular and Modified Triangular Plan Forms," NACA RM L8L29, March 1949.

[8]Jones, R., Miles, C. J. W., and Pusey, P. S., "Experiments in the Compressed Air Tunnel on Swept-Back Wings Including Two Delta Wings," British Aeronautical Research Council (A.R.C.) R. & M. 2871, 1954.